Electron Rearrangement Dynamics in Dissociating I_2^{n+} Molecules Accessed by Extreme Ultraviolet Pump-Probe Experiments

K. Schnorr,[1,*] A. Senftleben,[1] M. Kurka,[1] A. Rudenko,[2] G. Schmid,[1] T. Pfeifer,[1] K. Meyer,[1] M. Kübel,[3] M. F. Kling,[2,3] Y. H. Jiang,[4] R. Treusch,[5] S. Düsterer,[5] B. Siemer,[6] M. Wöstmann,[6] H. Zacharias,[6] R. Mitzner,[7] T. J. M. Zouros,[8] J. Ullrich,[9] C. D. Schröter,[1] and R. Moshammer[1]

[1]*Max-Planck-Institut für Kernphysik, 69117 Heidelberg, Germany*
[2]*J.R. Macdonald Laboratory, Kansas State University, Manhattan, Kansas 66506, USA*
[3]*Max-Planck-Institut für Quantenoptik, 85748 Garching, Germany*
[4]*Shanghai Advanced Research Institute, Chinese Academy of Sciences, Shanghai 201210, China*
[5]*Deutsches Elektronen-Synchrotron, 22607 Hamburg, Germany*
[6]*Westfälische Wilhelms-Universität, 48419 Münster, Germany*
[7]*Helmholtz-Zentrum Berlin, 12489 Berlin, Germany*
[8]*Department of Physics, University of Crete, Post Office Box 2208, 71003 Heraklion, Crete, Greece*
[9]*Physikalisch-Technische Bundesanstalt, 38116 Braunschweig, Germany*

(Received 7 March 2014; published 11 August 2014)

The charge rearrangement in dissociating I_2^{n+} molecules is measured as a function of the internuclear distance R using extreme ultraviolet pulses delivered by the free-electron laser in Hamburg. Within an extreme ultraviolet pump-probe scheme, the first pulse initiates dissociation by multiply ionizing I_2, and the delayed probe pulse further ionizes one of the two fragments at a given time, thus triggering charge rearrangement at a well-defined R. The electron transfer between the fragments is monitored by analyzing the delay-dependent ion kinetic energies and charge states. The experimental results are in very good agreement with predictions of the classical over-the-barrier model demonstrating its validity in a thus far unexplored quasimolecular regime relevant for free-electron laser, plasma, and chemistry applications.

DOI: 10.1103/PhysRevLett.113.073001 PACS numbers: 33.80.Rv, 32.80.Hd, 34.70.+e, 82.53.Eb

The dynamics of charge relaxation, rearrangement, and equilibration at the transition between chemically bound and unbound systems is essential for understanding many chemical [1,2] and plasma reactions [3,4]. It is also crucial for the imaging of biomolecules with atomic resolution, a key application of free-electron lasers (FELs). Here, the idea is to take a snapshot of the molecule by irradiating the system with intense ultrashort (< 100 fs) x-ray pulses before it is damaged [5]. Recent experiments on nanocrystalized lysozyme, however, have shown that the photon-induced damage leads to a scattering pattern that is different from what is expected for the intact molecule even for x-ray pulses as short as 70 fs [6]. Photon absorption is strongly localized at constituents with high atomic numbers, often having more than an order of magnitude larger cross sections as compared to H or even C atoms [7]. Therefore, it is crucial to understand the underlying ultrafast electronic and nuclear rearrangement dynamics in order to develop improved damage models that take into account the spatiotemporal spread of the locally induced charge.

Localized photon absorption efficiently triggers atomic movement and electron rearrangement across the entire molecular ion, mainly leading to its fragmentation. In a recent study, methylselenol [8] and ethylselenol [9] molecules, containing one heavy selenium atom as photoabsorption center, were irradiated with single intense 5 fs x-ray pulses. From the observed charge-state distributions and the fragments' kinetic energies, it could be concluded that even for such short pulses ultrafast charge rearrangement takes place, accompanied by considerable atomic displacements, which is relevant for imaging with atomic resolution. However, the central question concerning the underlying time and length scales remained open.

In this Letter, we present experimental results on the electron transfer between two iodine ions at freely chosen internuclear distances R. A dissociation of the I_2 molecule is triggered by multiple ionization with a femtosecond pump pulse [10]. The evolving system is then further ionized by the delayed probe pulse. Depending on the time delay, or the corresponding internuclear distance, and the charge states created by the pump pulse, an electron can be transferred from one constituent to the other, as illustrated in Fig. 1. We explicitly address the question of how fast and up to which critical distance R_{crit} charge can be rearranged. Our results are in excellent agreement with the predictions of the classical over-the-barrier (COB) model [11,12] that has been developed to describe charge transfer in ion-atom collisions.

The experiment was conducted at the beam line BL2 at the free-electron laser in Hamburg (FLASH), which is

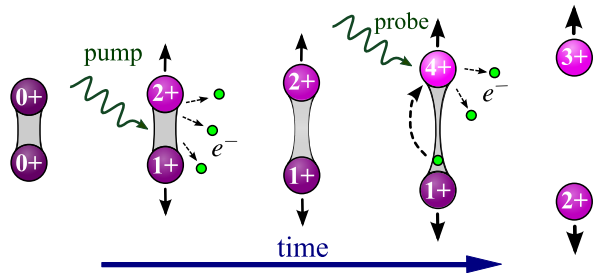

FIG. 1 (color online). Illustration of the XUV-pump–XUV-probe scheme. The pump pulse triggers the dissociation into $I^{1+} + I^{2+}$ by multiple ionization. The delayed probe pulse creates an I^{4+} ion that in turn attracts electrons from the other side of the molecule, resulting in the more symmetric breakup into $I^{2+} + I^{3+}$. Charge transfer is possible only up to a critical internuclear separation, beyond that the fragments behave as individual ions.

equipped with an autocorrelator that splits the incoming FEL beam geometrically into two equal parts and introduces an adjustable time delay between them to allow for extreme ultraviolet (XUV) pump-probe experiments [13]. The two beams are spatially overlapped and focused down to a diameter of approximately 35 μm. We used 87 eV pulses at a repetition rate of 300 pulses/s with a duration of approximately 60 fs (FWHM) and an intensity of roughly 10^{14} W/cm^2. The FEL beam was focused into a supersonic gas jet containing iodine molecules. In order to produce a gaseous iodine target, solid iodine was heated to 400 K inside a reservoir containing helium gas at a stagnation pressure of 1 bar, resulting in a $He:I_2$ ratio of approximately 50:1. The gas mixture was expanded through a heated 30 μm diameter nozzle to create a supersonic jet.

By means of a reaction microscope [14], we detected all coincident ionic fragments created upon ionization. The ions were accelerated by a homogeneous electric field of 35 V/cm onto a time- and position-sensitive detector, which allowed us to reconstruct the initial three-dimensional momenta and the charge states. During the measurement, the pump-probe delay time was continuously scanned between -2 and $+2$ ps, meaning that one of the pulses precedes the other for negative delays and succeeds it for positive delays.

We first consider the ionization with a single photon of 87 eV. This energy is close to the maximum of the $4d$ giant shape resonance in I_2 [15], which amounts to more than 80% of the total cross section [16]. Thus, absorption of one photon mostly leads to the creation of a $4d$-type vacancy that undergoes either a single Auger decay ($A1$) leading to I_2^{2+} or a cascade of two Auger processes ($A1 + A2$) resulting in I_2^{3+} [10]. $A1$ has a lifetime of only a few femtoseconds [17], while the decay time of $A2$ was determined recently to be 23 fs [18]. Two singly charged iodine ions that repel each other by the Coulomb force expand within 150 fs to twice their equilibrium internuclear distance. Thus, $A1$ and $A2$ can be considered fast compared to both the FEL pulse duration and the dissociation time. In a low-intensity measurement at FLASH, we detected only a small fraction of bound I_2^{2+} (< 10%) and I_2^{3+} (< 1%) as the majority of molecular ions dissociates. Hence, the absorption of a single 87 eV photon mainly leads to the creation of dissociating I_2^{2+} or I_2^{3+} molecular ions that fragment into

$$I_2 \xrightarrow{h\nu} I_2^{*+} \xrightarrow{A1+A2} I_2^{3+} \longrightarrow I^{1+} + I^{2+} \quad (55\%), \tag{1}$$

$$I_2 \xrightarrow{h\nu} I_2^{*+} \xrightarrow{A1} I_2^{2+} \longrightarrow I^{1+} + I^{1+} \quad (44\%), \tag{2}$$

$$I_2 \xrightarrow{h\nu} I_2^{*+} \xrightarrow{A1} I_2^{2+} \longrightarrow I + I^{2+} \quad (< 1\%). \tag{3}$$

At the higher intensity of 10^{14} W/cm^2, multiple photons are absorbed within one pulse: Using Xe gas as a target that also features a $4d$ shape resonance [19], analog to the one in I_2, we observed charge states up to Xe^{6+}, the highest one that can be produced by a sequence of at least four single-photon ionization events. With identical beam parameters, I_2^{12+} was reached, allowing us to draw the same conclusion that mostly sequential single-photon absorption took place. Thus, the first photon produces I_2^{2+} or I_2^{3+}, the second one creates another $4d$-type vacancy with a subsequent Auger decay resulting in I_2^{4+} or I_2^{5+}, respectively [20], and the third one photoionizes the aforementioned molecular ions.

With this knowledge we now discuss the results obtained with two consecutive intense XUV pulses. The delay-dependent kinetic energy release (KER) for the fragmentation channel $I^{2+} + I^{3+}$ is shown in Fig. 2(a). In the following, coincident ions will be denoted as (P, Q) instead of $I^{P+} + I^{Q+}$. Figure 2(a) shows two distinct features, a constant one around 27 eV and a delay-dependent trace converging to 11 eV [Figs. 2(a) and 2(b)]. The constant feature emerges from two-photon absorption within one pulse, as can be shown by evaluating the KER. Assuming purely Coulombic potential energy curves, the KER can be estimated via $\mathrm{KER} \approx E_{\mathrm{Coul}} = (P \cdot Q)/R$ (atomic units, a.u., are used throughout). Thus, for the instantaneous ionization $I_2 \rightarrow (2,3)$ at equilibrium internuclear distance $R_{\mathrm{eq}} = 5$ a.u., the expected KER amounts to 32 eV. The disagreement with the measured value of 27 eV hints toward an ultrafast increase of the distance R between the constituents: In order to produce I_2^{5+}, that eventually breaks into (2,3), two photons are required. Since these photons will be absorbed sequentially within the same pulse, the first photon triggers the dissociation leading to an increased R by the time the second photon creates an ion pair with charges (2,3).

The time-dependent KER traces overlap for small delays with the single pulse case [Fig. 2(a)], because the pump and probe pulses can be considered as one pulse within their temporal overlap. With increasing delay, the KER gets

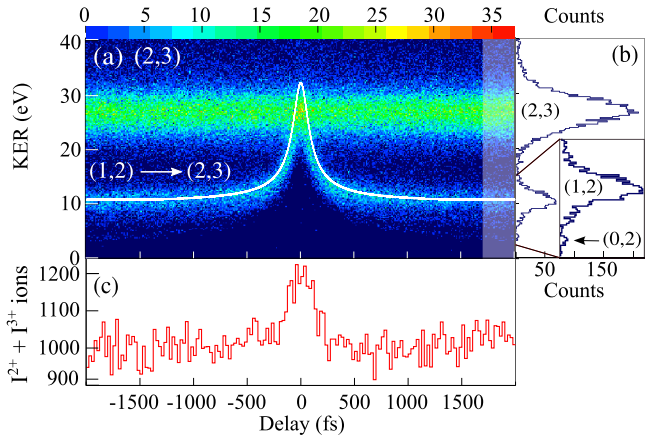

FIG. 2 (color online). (a) KER for all coincident (2,3) ion pairs plotted as a function of the time delay. The classical simulation via the pathway $(1,2) \rightarrow (2,3)$ is superimposed in white. (b) Projection of KERs at large delays (shaded area) onto the KER axis with the inset showing a magnified view of the low-energy region. The charge states belonging to the observed asymptotic KERs are indicated in brackets. (c) Projection of all KERs onto the delay axis.

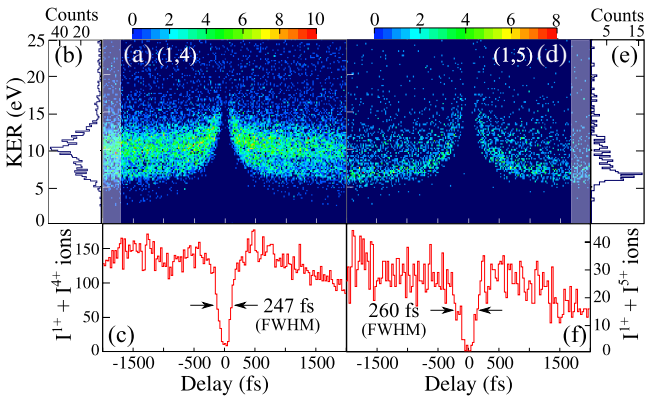

FIG. 3 (color online). (a), (d) Delay-dependent KER spectra of all coincident (1,4) (a) and (1,5) (d) ion pairs. (b),(e) Projection of KERs at large delays (shaded area) onto the KER axis. (c),(f) Projection of all KERs onto the delay axis. For delays below (124 ± 3) fs (HWHM) no coincident (1,4) ions are detected, while for (1,5) the corresponding range of delays is (130 ± 5) fs (HWHM).

smaller, finally converging to an asymptotic value of 11 eV [Fig. 2(b)]. This is due to the creation of intermediate charge states $(P_i,\ Q_i)$ by the pump pulse leading to dissociation until the probe pulse promotes the system onto a steeper potential energy curve belonging to the final charge states $(P_f,\ Q_f)$. The longer the delay, the smaller the energy gain gets on the steeper curve. For very large delays the measured KER is equal to that of the precursor state $(P_i,\ Q_i)$. This allows us to reconstruct the reaction pathway leading to the final coincidence channel $(P_f,\ Q_f)$. Therefore, an asymptotic KER of 11 eV in Fig. 2(b), corresponding to the Coulomb energy of an I^+ and an I^{2+} ion at R_{eq}, suggests the pathway $I_2 \xrightarrow{\mathrm{pump}} (1,2) \xrightarrow{\mathrm{probe}} (2,3)$.

To substantiate this interpretation, we use a Coulomb-explosion model in which we treat the ions classically as moving pointlike charges: The equation of motion is solved for a particle with the reduced mass $\mu = m_{\mathrm{iodine}}/2$ in a potential $(P \cdot Q)/R$. The dissociation initiated by the pump pulse is modeled by placing the system onto the intermediate potential $(P_i \cdot Q_i)/R$ at R_{eq} with zero initial velocity and following the motion for all internuclear distances R. The ionization by the probe pulse is assumed to be instantaneous, promoting the molecular ion onto the steeper $(P_f \cdot Q_f)/R$ potential. The propagation is continued until an asymptotic KER value is reached. The result of the simulation for the channel (2,3) via the precursor (1,2) is shown in Fig. 2(a) in white. Very good agreement with the experiment is obtained supporting the proposed pathway and the use of purely Coulombic potentials.

The coincidence channel (1,4) with two overlapping traces of precursor states is shown in Fig. 3(a). The dominant trace converging to roughly 11 eV [Fig. 3(b)] can be identified as emerging from the precursor charge state (1,2): $I_2 \xrightarrow{\mathrm{pump}} (1,2) \xrightarrow{\mathrm{probe}} (1,4)$. The weak trace converging to approximately 6 eV stems from single-photon absorption within the pump pulse initiating the dissociation via the precursor (1,1), which is further ionized by two photons from the probe pulse leading to (1,4): $I_2 \xrightarrow{\mathrm{pump}} (1,1) \xrightarrow{\mathrm{probe}} (1,4)$. As the latter pathway requires two-photon absorption within one pulse, it is considerably weaker than the single-photon pathway.

Striking differences between the equally charged channels (1,4) and (2,3) are found for small delays [Fig. 3(c) and Fig. 2(c), respectively]. The yield of the (1,4) channel vanishes almost completely for overlapping pulses and no time-independent trace appears, meaning that these charge states are not created within a single pulse. Another asymmetric channel (1,5) [Fig. 3(d)], mainly produced via the precursor (1,1), shows similar features, in particular, the depleted ion yield at small delays [Fig. 3(f)].

According to their characteristic time dependences, all observed coincidence channels can be grouped into two classes. Asymmetrically charged fragments with $|P - Q| > 1$ exhibit a pronounced yield minimum at small delays while symmetric ones do not. In particular, many of the symmetric channels even show a maximum of the count rate at small delays [Fig. 2(c)]. This is expected because a more positive charge at one of the ions will attract electrons throughout the molecule, and due to the very fast electronic motion, the rearrangement of charges will favor a symmetric breakup. Thus, any charge asymmetry induced by the probe pulse is effectively equalized. This is valid for small delays corresponding to small internuclear distances. Beyond a critical value R_{crit} the two individual ionic fragments respond as if they were isolated instead of belonging to a molecular system; i.e., all charges will

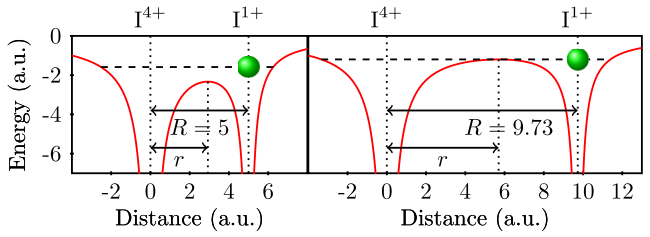

FIG. 4 (color online). Illustration of the COB model for the coincidence channel (1,4). At $R_{\mathrm{eq}} = 5$ a.u., the most loosely bound electron ($E_{P_f} = -19.2$ eV [21]) can easily overcome the potential barrier toward I^{4+} while electron transfer is blocked beyond $R_{\mathrm{crit}} = 9.73$ a.u.

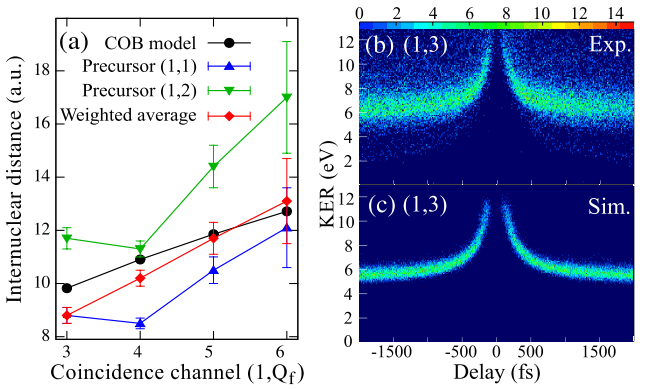

FIG. 5 (color online). (a) R_{crit} as a function of the asymmetric coincidence channel (1, Q_f) with $Q_f \in \{3,4,5,6\}$. The black circles show the predictions from the COB model $R_{\mathrm{crit}}^{\mathrm{COB}}$ with $E_{P_f} = -19.2$ eV [21], while the experimental data $R_{\mathrm{crit}}^{\mathrm{exp}}$ for the precursor (1,1) are drawn as blue upward triangles, those for (1,2) as green downward triangles, and the weighted average as red diamonds. (b) Delay-dependent KER for (1,3). (c) Simulation of the delay-dependent KER for (1,3) with a finite pulse length of 57 fs (FWHM) and a width for the spatial ground-state distribution of 0.5 a.u. (FWHM).

remain localized at the nuclei. Thus, by varying the time delay between the two pulses and monitoring the charge states of the ionic fragments, the critical times and the corresponding R_{crit} up to which charge transfer occurs can be determined.

To obtain a more quantitative picture of the charge rearrangement dynamics or a measure for the critical internuclear distance R_{crit}, we use the COB model to describe the electron transfer from one ion to the other. We consider two ions I^{P_f} and I^{Q_f} with $P_f \leq Q_f$ that are separated by R. A purely one-dimensional model is used where the connection line between the two nuclei forms the coordinate axis. The binding energy $E_{P_f} < 0$ of the least bound electron of I^{P_f} is increased by the presence of the charge Q_f to $E'_{P_f} = E_{P_f} - Q_f/R$. The outermost electron of I^{P_f}, located at r, experiences a potential $V_e(r,R)$ that results from the superposition of the Coulomb potential of its own nucleus with effective charge $P_f + 1$ and that of the neighboring ion with Q_f,

$$V_e(r,R) = -\frac{P_f + 1}{R - r} - \frac{Q_f}{r}. \tag{4}$$

The electron can classically cross over to I^{Q_f} as long as its binding energy E'_{P_f} lies above the potential barrier as indicated in Fig. 4 for $(P_f, Q_f) = (1,4)$. Charge transfer is not possible for internuclear distances larger than

$$R_{\mathrm{crit}} = \frac{P_f + 1 + 2\sqrt{(P_f + 1)Q_f}}{|E_{P_f}|}. \tag{5}$$

R_{crit} can be predicted for all asymmetric charges via Eq. (5). However, in the experiment a critical time delay t_{crit} is measured, which is determined by the half width at half minimum (HWHM) of the dip observed in KER traces [compare Figs. 3(c) and 3(f)]. t_{crit} can be translated into R_{crit} by calculating the nuclear dynamics of the molecule between the two pulses. This is done using our classical pump-probe simulation, which assumes a purely Coulombic potential defined by the intermediate charge states P_i and Q_i. However, in the experiment t_{crit} cannot be attributed to a specific precursor state due to resolution and statistical limitations. Since all considered coincidence channels contain at least one of the main precursors (1,1) and (1,2), we calculate $R_{\mathrm{crit}}^{\mathrm{exp}}$ for (1,1) [Fig. 5(a), blue upward triangles] and for (1,2) [Fig. 5(a), green downward triangles].

All $R_{\mathrm{crit}}^{\mathrm{COB}}$ values predicted by the COB model [Fig. 5(a), black circles] lie between the corresponding experimental data points $R_{\mathrm{crit}}^{\mathrm{exp}}$ via the precursor states (1,1) and (1,2). Notably, for the (1,4) channel $R_{\mathrm{crit}}^{\mathrm{COB}}$ shows a tendency toward $R_{\mathrm{crit}}^{\mathrm{exp}}$ via (1,2), which is also the main precursor observed in the experiment. As another example, the (1,5) channel evolves mostly from (1,1). Also, here the corresponding critical distance from the COB model tends toward $R_{\mathrm{crit}}^{\mathrm{exp}}$ via (1,1). These trends encourage us to calculate average experimental values $\bar{R}_{\mathrm{crit}}^{\mathrm{exp}}$, where we weight $R_{\mathrm{crit}}^{\mathrm{exp}}$ via (1,1) and (1,2) according to the number of counts contained in the respective precursor trace. The resulting values [Fig. 5(a), red diamonds] are in very good agreement with the prediction of the COB model.

As a next step we extend our Coulomb-explosion simulation by introducing a finite pulse duration and combining it with the COB model to reproduce the time-dependent KER spectra. The FEL pulse duration is estimated from the width of the time-dependent trace in Fig. 2(a): As the width is mostly dependent on the pulse duration and the populated ground-state vibrational levels, the latter being small and identical for all pulse parameters, the pulse duration is the critical parameter influencing the width of the trace at small delays. By projecting a thin slice of KERs around 19 eV from Fig. 2(a) onto the delay axis and assuming that pump and probe pulse have the same

duration, an upper limit of 57 fs (FWHM) for the pulse duration is extracted. Figure 5 shows the comparison of experimental data for the channel (1,3) [Fig. 5(b)] with the result of the simulation via the precursor (1,1) and Gaussian pulses of 57 fs [Fig. 5(c)]. The excellent agreement demonstrates that classical models are suitable to describe both the dissociation dynamics and charge rearrangement in highly charged molecules.

It should be noted that the COB model used here is analog to those applied for field ionization in strong laser fields (e.g., [22,23]) and slow ion-atom collisions [11,12]. Our experimental situation is similar to a collision, with the difference that now the reaction partners start from their closest distance. This way the ionic fragments are always emitted back to back and the motion is limited to one dimension as assumed in the COB model [24]. In addition, the classical treatment is justified only for small projectile velocities such that the electronic states can adjust adiabatically to the changing potentials. For dissociating I_2^{n+}, with ion kinetic energies below 0.1 eV per nucleon, this condition is very well fulfilled. Our experiment thus represents the ideal testing ground of the COB model at very low energies typical for chemical reactions.

In summary, the electron transfer dynamics between two iodine ions emerging from the breakup of I_2^{n+} is studied as a function of their separation. This is experimentally realized by inducing dissociation of an I_2 molecule by means of an XUV pump pulse and creating a charge asymmetry by an XUV probe pulse. By mapping the delay-dependent kinetic energies of the ions along with their final charge states, the complete fragmentation pathway including the intermediate degree of ionization after the pump pulse becomes accessible. This allows us to determine the critical internuclear distance up to which electron transfer occurs. The experimental data are in excellent agreement with the classical over-the-barrier model for electron exchange. The results demonstrate that electron rearrangement may proceed over large distances of 10 a.u. or more, and that charges created locally within a molecule by, e.g., absorption of x rays at a heavy atomic constituent are very effectively distributed over the whole system within a time that is much shorter than the dissociation time. It leads to an overall acceleration of molecular damage, a critical quantity in FEL scattering experiments.

We acknowledge technical support from B. Knape and C. Kaiser, and thank the scientific and technical team at FLASH for optimal beam conditions. A. R. acknowledges support from Kansas NSF EPSCoR "First Award" Program. A. R. and M. F. K. are grateful for support by the U.S. Department of Energy under DE-FG02-86ER13491, M. K. and M. F. K. acknowledge support by the DFG via the Cluster of Excellence: Munich Center for Advanced Photonics. Y. H. J. is grateful for support from the NSFC (Grant No. 11274232), the National Basic Research Program of China (973 Program) (Grant No. 2013CB922200), and the Shanghai Pujiang Program (Grant No. 13PJ1407500).

*Kirsten.Schnorr@mpi-hd.mpg.de

[1] Z. Herman, Int. Rev. Phys. Chem. **15**, 299 (1996).
[2] Z. Deng, I. Bald, E. Illenberger, and M. A. Huels, Phys. Rev. Lett. **96**, 243203 (2006).
[3] G. Lubinski, Z. Juhász, R. Morgenstern, and R. Hoekstra, Phys. Rev. Lett. **86**, 616 (2001).
[4] D. Bodewits, D. J. Christian, M. Torney, M. Dryer, C. M. Lisse, K. Dennerl, T. H. Zurbuchen, S. J. Wolk, A. G. G. M. Tielens, and R. Hoekstra, Astron. Astrophys. **469**, 1183 (2007).
[5] R. Neutze, R. Wouts, D. van der Spoel, E. Weckert, and J. Hajdu, Nature (London) **406**, 752 (2000).
[6] L. Lomb *et al.*, Phys. Rev. B **84**, 214111 (2011).
[7] J. Yeh and I. Lindau, At. Data Nucl. Data Tables **32**, 1 (1985).
[8] B. Erk *et al.*, Phys. Rev. Lett. **110**, 053003 (2013).
[9] B. Erk *et al.*, J. Phys. B **46**, 164031 (2013).
[10] B. H. Boo and N. Saito, J. Electron Spectrosc. Relat. Phenom. **127**, 139 (2002).
[11] H. Ryufuku, K. Sasaki, and T. Watanabe, Phys. Rev. A **21**, 745 (1980).
[12] A. Niehaus, J. Phys. B **19**, 2925 (1986).
[13] M. Wöstmann, R. Mitzner, T. Noll, S. Roling, B. Siemer, F. Siewert, S. Eppenhoff, F. Wahlert, and H. Zacharias, J. Phys. B **46**, 164005 (2013).
[14] J. Ullrich, R. Moshammer, A. Dorn, R. Dörner, L. P. H. Schmidt, and H. Schmidt-Böcking, Rep. Prog. Phys. **66**, 1463 (2003).
[15] F. J. Comes, U. Nielsen, and W. H. E. Schwarz, J. Chem. Phys. **58**, 2230 (1973).
[16] J. Tremblay, M. Larzilliere, F. Combet-Farnoux, and P. Morin, Phys. Rev. A **38**, 3804 (1988).
[17] J. N. Cutler, G. M. Bancroft, and K. H. Tan, J. Chem. Phys. **97**, 7932 (1992).
[18] M. Krikunova, T. Maltezopoulos, P. Wessels, M. Schlie, A. Azima, M. Wieland, and M. Drescher, J. Chem. Phys. **134**, 024313 (2011).
[19] A. A. Sorokin, S. V. Bobashev, T. Feigl, K. Tiedtke, H. Wabnitz, and M. Richter, Phys. Rev. Lett. **99**, 213002 (2007).
[20] H. Kjeldsen, P. Andersen, F. Folkmann, H. Knudsen, B. Kristensen, J. B. West, and T. Andersen, Phys. Rev. A **62**, 020702 (2000).
[21] M. Eypper, F. Innocenti, A. Morris, J. M. Dyke, S. Stranges, J. B. West, and G. C. King, J. Chem. Phys. **133**, 084302 (2010).
[22] J. H. Posthumus, A. J. Giles, M. R. Thompson, and K. Codling, J. Phys. B **29**, 5811 (1996).
[23] M. Krikunova, T. Maltezopoulos, P. Wessels, M. Schlie, A. Azima, T. Gaumnitz, T. Gebert, M. Wieland, and M. Drescher, Phys. Rev. A **86**, 043430 (2012).
[24] J. Burgdörfer, R. Morgenstern, and A. Niehaus, J. Phys. B **19**, L507 (1986).